

# Continuous wave quantum cascade lasers with 5.6 W output power at room temperature and 41% wall-plug efficiency in cryogenic operation

Cite as: AIP Advances 10, 055120 (2020); <https://doi.org/10.1063/5.0003318>

Submitted: 31 January 2020 • Accepted: 06 May 2020 • Published Online: 19 May 2020

F. Wang, S. Slivken,  D. H. Wu, et al.

## COLLECTIONS

Paper published as part of the special topic on [Photonics and Optics](#)



View Online



Export Citation



CrossMark

## ARTICLES YOU MAY BE INTERESTED IN

[Room temperature quantum cascade laser with ~ 31% wall-plug efficiency](#)

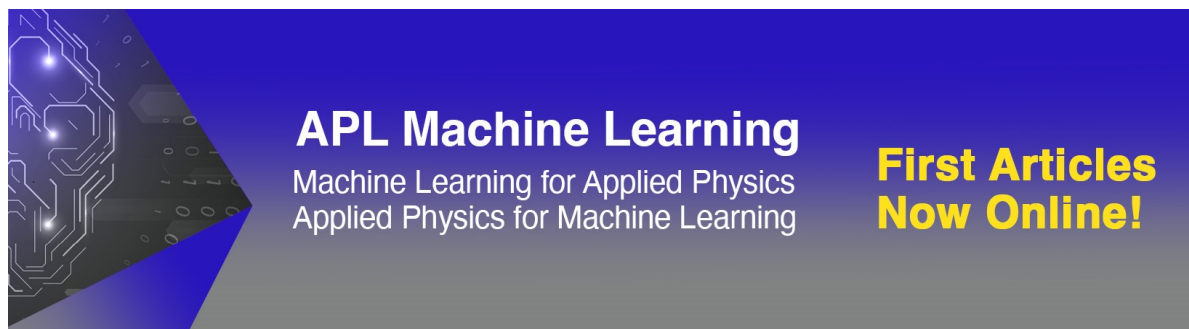
AIP Advances 10, 075012 (2020); <https://doi.org/10.1063/5.0012925>

[Room temperature quantum cascade lasers with 27% wall plug efficiency](#)

Applied Physics Letters 98, 181102 (2011); <https://doi.org/10.1063/1.3586773>

[Highly temperature insensitive quantum cascade lasers](#)

Applied Physics Letters 97, 251104 (2010); <https://doi.org/10.1063/1.3529449>



**APL Machine Learning**  
Machine Learning for Applied Physics  
Applied Physics for Machine Learning

**First Articles  
Now Online!**

# Continuous wave quantum cascade lasers with 5.6 W output power at room temperature and 41% wall-plug efficiency in cryogenic operation

Cite as: AIP Advances 10, 055120 (2020); doi: 10.1063/5.0003318

Submitted: 31 January 2020 • Accepted: 6 May 2020 •

Published Online: 19 May 2020



F. Wang, S. Slivken, D. H. Wu,  Q. Y. Lu, and M. Razeghi<sup>a)</sup> 

## AFFILIATIONS

Center for Quantum Devices, Department of Electrical and Computer Engineering, Northwestern University, Evanston, Illinois 60208, USA

<sup>a)</sup>Author to whom correspondence should be addressed: [razeghi@northwestern.edu](mailto:razeghi@northwestern.edu)

## ABSTRACT

In this paper, we report a post-polishing technique to achieve nearly complete surface planarization for the buried ridge regrowth processing of quantum cascade lasers. The planarized device geometry improves the thermal conduction and reliability and, most importantly, enhances the power and efficiency in continuous wave operation. With this technique, we demonstrate a high continuous wave wall-plug efficiency of an InP-based quantum cascade laser reaching ~41% with an output power of ~12 W from a single facet operating at liquid nitrogen temperature. At room temperature, the continuous wave output power exceeds the previous record, reaching ~5.6 W.

© 2020 Author(s). All article content, except where otherwise noted, is licensed under a Creative Commons Attribution (CC BY) license (<http://creativecommons.org/licenses/by/4.0/>). <https://doi.org/10.1063/5.0003318>

The quantum cascade laser (QCL) is a unipolar quantum device fully based on a semiconductor technology platform.<sup>1,2</sup> It is compact and electrically pumped, and the “band structure-by-design” nature allows its frequency and bandwidth to be tailorable from mid-infrared to terahertz (THz) ranges.<sup>3,4</sup> In such a laser system, wall-plug efficiency (WPE) is the energy conversion efficiency with which the QCL converts electrical power into optical power. It is of great importance to optimize the WPE as it can, on the one hand, maximize the useful energy of a QCL and, on the other hand, reduce the heat produced within the laser system. This can significantly improve device reliability, especially for QCLs under continuous wave (cw) operation. Since cw QCLs with high output power and high WPE are desired for a plethora of pivotal applications in industry, constant effort has been devoted to this research domain worldwide during the past 20 years. Recently, mid-infrared QCLs have undergone considerable developments in terms of output power and efficiency, which include watt-level cw power output at  $\lambda = 3.7 \mu\text{m}$ , an 8.2 W phased array demonstration at  $\lambda = 8 \mu\text{m}$ ,<sup>5,6</sup> and the demonstration of cw WPE up to 21% with an output power

beyond ~5 W from a buried ridge device at room-temperature.<sup>7</sup> This record has been held for almost a decade. This is partially because the global optimization of all the involved laser parameters is tricky and the growth of a high-quality QCL active region is challenging. While the WPE in the pulsed mode can be readily enhanced by increasing the band offset in the active region to suppress the carrier leakage into the continuum, the increased strain by adjusting the material compositions results in a reduced differential gain of 2.7 cm/kA.<sup>8</sup> This negatively impacts performance when a narrow waveguide width is applied for cw operation. Before entering the comprehensive optimization procedure to the active region, which involves many rounds of design, growth, fabrication, and testing, we were focused on the fabrication process optimization to evaluate possible improvement to the device performance. Here, we redesign the buried ridge regrowth process and introduce a post-polishing technique to achieve better surface planarization and improve the device reliability and performance. High continuous wave WPE up to ~41% at 80 K and high cw output power up to 5.6 W at room temperature are demonstrated.

The buried ridge regrowth process has been widely used in the fabrication of high-power cw QCLs.<sup>9</sup> After the formation of a laser ridge waveguide by wet etching two channels ( $\sim 10\ \mu\text{m}$  deep) on either side, the regrowth of semi-insulating Fe:InP cladding is performed by metalorganic chemical vapor deposition (MOCVD) to fill the channels. This will significantly reduce the optical loss and increase the thermal conductivity. Ideally, a complete planarization of the channels is desired to suppress any losses due to the processing. However, the planarization is difficult to achieve since the regrowth rate depends on many factors, including the opening width, volume of the channels, and density of the channel patterns. Overgrowth of Fe:InP is generally undesired because it would introduce thermal dissipation issues to devices bonded epilayer-down to a heat sink. Therefore, for past efforts, the channels were undergrown with  $1\text{--}3\ \mu\text{m}$  depth unfilled. This type of undergrowth for the devices can introduce air gaps in the channels during epi-layer down bonding, which will result in less effective heat dissipation for cw operation. Here, we redesign the buried ridge regrowth process and introduce a post-polishing technique, as the schematic shown in Fig. 1(a). Instead of undergrowth, the etched channels are intentionally overgrown by  $3\text{--}5\ \mu\text{m}$  to completely fill the empty channel. The  $1\text{-}\mu\text{m}$  thick  $\text{SiO}_2$  layer, which has been used as the hard mask for the regrowth, will be used as the protecting layer during the post-polishing treatment. This polishing step will not only

flatten the overgrown channels but also remove any defects on top of the mask generated during the Fe:InP regrowth, which might later turn into failure spots after packaging. Figures 1(b) and 1(c) show the scanning electron microscope (SEM) images of a typically undergrown device and a completely planarized device (upper panels) and their thermal distribution (lower panels) under a power density of  $1.3 \times 10^{14}\ \text{W/m}^3$  near the cw threshold. Clearly, the epilayer-down bonded, planarized device exhibits an internal temperature of  $5^\circ\text{C}$  lower than that of the undergrown device. This is attributed to the improved thermal contact for the planarized device. As the current increases, this temperature discrepancy will increase as well. As a result, the planarized device would exhibit improved reliability and performance compared with the undergrown devices.

The band structure of the QCL gain medium is based on the shallow-well design in Ref. 7, with the average laser core doping level adjusted to be  $1.8 \times 10^{16}\ \text{cm}^{-3}$ . Although the reduced doping will limit the current dynamic range, it can bring a lower threshold current density and lower waveguide loss, both of which favor cw operation of QCLs. Similar to Ref. 7, the QCL wafer was grown in a gas-source molecular beam epitaxy (gsMBE) reactor on a  $n$ -InP substrate and ended with a  $3\text{-}\mu\text{m}$  low doped ( $2 \times 10^{16}\text{--}2 \times 10^{17}\ \text{cm}^{-3}$ ) InP cladding layer and a  $1\text{-}\mu\text{m}$  highly doped ( $1 \times 10^{19}\ \text{cm}^{-3}$ ) InP cap layer. After standard material characterization, the

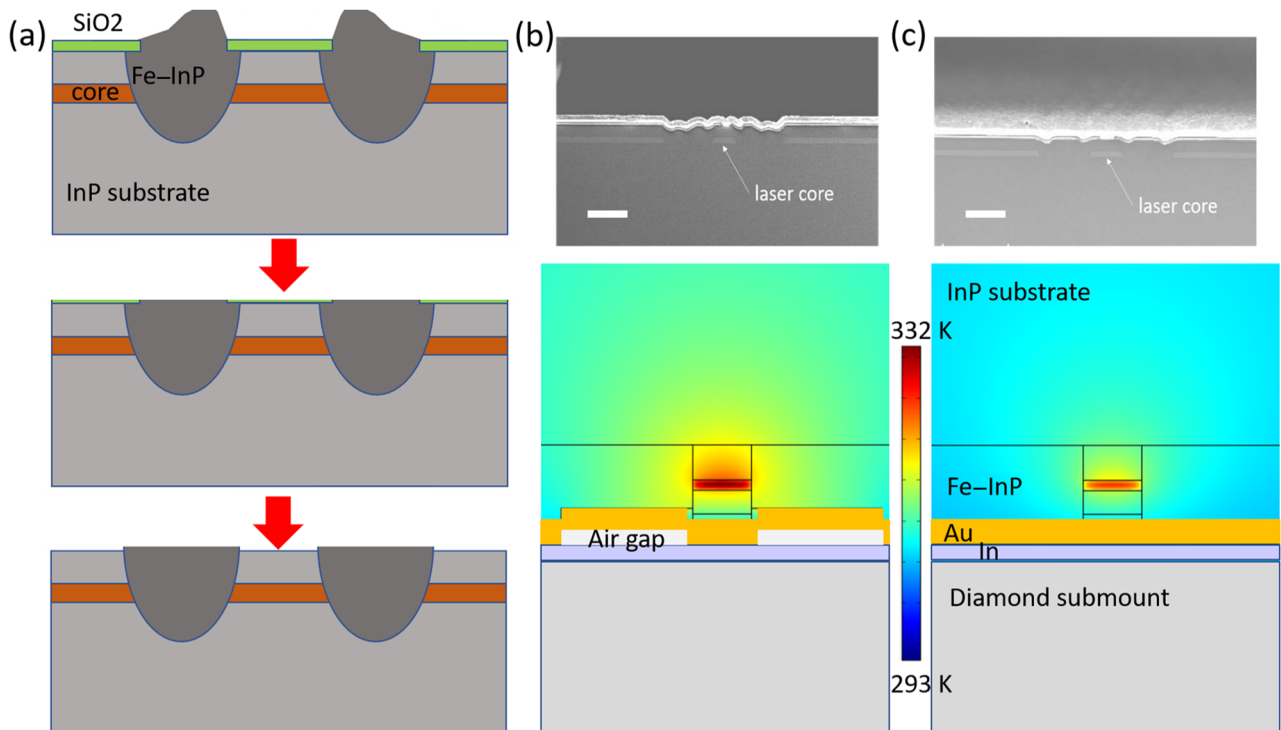


**FIG. 1.** (a) Schematic of the processing flow for the redesigned buried ridge process. (b) The SEM image of an epilayer-down bonded undergrown QCL device (upper panel) and the device thermal distribution simulated with the finite-element method (lower panel). (c) The SEM image of an epi-down bonded planarized QCL device using the redesigned processing technique (upper panel) and the thermal simulation result of the device (lower panel). The two simulation figures share the same scalar bar to reflect the internal temperature difference for the two cases. The white bars on the SEM images represent a length scale of  $10\ \mu\text{m}$ .

wafer was processed into buried ridge waveguide lasers with ridge widths 10  $\mu\text{m}$  and 11.6  $\mu\text{m}$ . Without additional mention, the QCLs used in this paper were cleaved to be 5-mm long. Their back facets were high reflectivity (HR) coated using  $\text{Y}_2\text{O}_3/\text{Au}/\text{Ti}$ , and the front facets were anti-reflectivity (AR) coated using  $\text{Y}_2\text{O}_3$ . A thickness of 360-nm  $\text{Y}_2\text{O}_3$  was used for the AR coating to make the total mirror loss equivalent to a 5-mm uncoated laser. To efficiently extract heat from the laser cores, the QCLs were epilayer-down bonded on patterned diamond heat spreaders using indium as the soldering material. Experiments were conducted in a cryostat from 80 K to 280 K and on a thermoelectric cooler (TEC) stage or microcooler at room temperature and above.

A comparison of optical power density and voltage as a function of current density ( $P$ - $J$ - $V$ ) for the two devices was performed and is shown in Fig. 2. Owing to the different ridge widths (10  $\mu\text{m}$  and 11.6  $\mu\text{m}$  for the two devices), the output power is converted into power density with respect to the ridge width. The  $P$ - $J$  curves in the pulsed mode (pulse width = 500 ns and repetition rate = 40 kHz) almost overlap each other for the two devices, as shown in Fig. 2(a). This is expected since the generated heat is nearly negligible in pulsed mode operation. However, the two devices behave differently in cw operation. The planarized device exhibits a reduced threshold density from 1.22  $\text{kA}/\text{cm}^2$  to 1.16  $\text{kA}/\text{cm}^2$  and improved maximum output power density from 0.42  $\text{W}/\mu\text{m}$  to 0.48  $\text{W}/\mu\text{m}$  [Fig. 2(b)]. This is attributed to the improved thermal conductivity of the planarized device over the undergrown device.

Regardless of the operating temperature, achieving high WPE and high cw power is always interesting since it can provide new inspiration for some extremely high-power applications that cannot be achieved by current lasers at room temperature. Previously, high WPE over 53% has been realized by using a single-well injector design.<sup>10</sup> However, the cw performance is not as impressive as the pulsed mode results, partially because of the lower  $T_0 \sim 120$  K of the design. Here, we studied power and WPE under different temperature conditions for the high-performance planarized QCL device. Figure 3(a) shows the light-current-voltage (LIV) curves of a 5-mm-long HR-AR coated QCL from 80 K to 373 K. From these curves, the

temperature dependent threshold current density (red circles), slope efficiency (black squares), WPE (blue circles), and resistance (orange circles) can be acquired, as shown in Fig. 3(b). The laser threshold current density can be fitted using  $J_{th}(T) = J_0 \exp(T/T_0)$ , where  $T$  is the operation temperature,  $T_0$  is the characteristic temperature, and  $J_0$  is the threshold current density at 0 K. By fitting the threshold current density data, the characteristic temperature of  $T_0 = 222$  K and current density of  $J_0 = 0.32$   $\text{kA}/\text{cm}^2$  are obtained. This  $T_0$  value is close to that in Ref. 7. Since the focus of the active region design in this work is to achieve high efficiency,  $T_0$  is not fully optimized compared with the highly temperature insensitive QCLs,<sup>11–15</sup> but it is still much higher than the device demonstrated with slightly higher pulsed WPE in Refs. 8 and 10. This is a strong indication that our laser will have superior performance in cw operation. Decreasing the temperature from 120 K to 80 K, the slope efficiency (SE) of the QCL under study seems unchanged or even slightly decreased, similar to what was observed for other QCL designs,<sup>16</sup> but the resistance dramatically increased by more than 30%, indicating that lower temperature does not necessarily give higher WPE. This is in agreement with the temperature dependent WPE in Fig. 3(b), where the maximum WPE is found to be situated at  $T_{max} \sim 120$  K, instead of 80 K. From 120 K up to 373 K, the SE decreases slowly with temperature increase due to enhanced non-radiative emission and reduced transport efficiency. The resistance also slowly decreases with the temperature increase from 80 K to 160 K, while above 250 K, it keeps almost constant owing to full ionization of electrons from doping impurities, as shown in Fig. 3(b).

The planarized QCL device was further investigated at 80 K and 293 K in cw operation. Together with the pulsed mode data, the results are summarized in Fig. 4. At room temperature (red), the threshold current densities of the QCL are 1.16  $\text{kA}/\text{cm}^2$  (cw) and 1.10  $\text{kA}/\text{cm}^2$  (pulsed), respectively. Compared with Ref. 7 (1.35  $\text{kA}/\text{cm}^2$  and 1.25  $\text{kA}/\text{cm}^2$ ), the smaller threshold difference (even with a wider ridge width) between cw and pulsed operation reveals the excellent thermal conduction of the planarized processing. In pulsed mode operation, the output power is  $\sim 10.7$  W with a maximum WPE of  $\sim 27\%$ . More importantly, in cw operation, the QCL delivers more than  $\sim 5.6$  W optical power at room

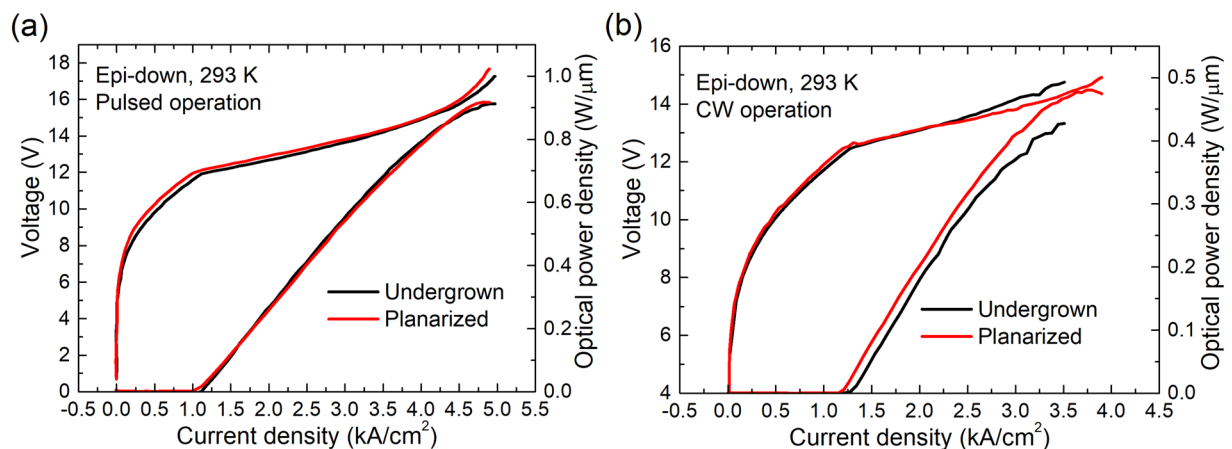
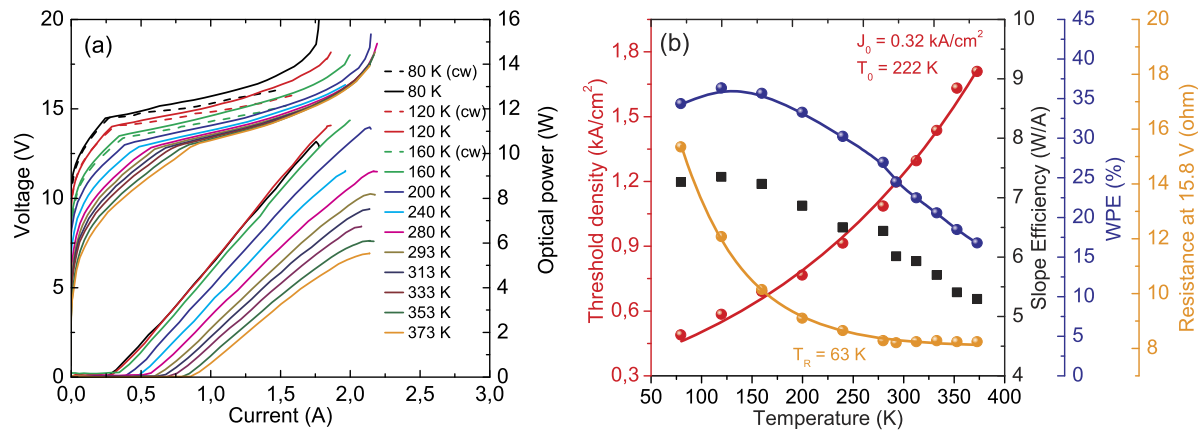


FIG. 2.  $P$ - $J$ - $V$  characterizations for the two QCLs with undergrowth and complete planarization in pulsed mode operation (a) and in continuous wave operation (b).



**FIG. 3.** (a) The temperature dependent light–current–voltage (LIV) curves of a QCL from 80 K to 373 K. (b) The temperature dependent threshold current density (red circles), slope efficiency (black squares), WPE (blue circles), and resistance (orange circles) of the QCL. This testing was conducted in the pulsed mode with a pulse width of 500 ns and a duty cycle of 2%.

temperature, exceeding the current record of  $\sim 5.1 \text{ W}$  by  $\sim 10\%$ . The emission wavelength of this laser is centered at  $\sim 4.97 \mu\text{m}$  at room temperature under cw operation at a driving current of  $\sim 0.8 \text{ A}$  [see Fig. 4(a), the red inset]. Multiple lasers have been tested, and repeated performance has been observed. This improved device reliability is attributed to the planarization technique during the Fe–InP regrowth processing.

The maximum pulsed WPE was obtained at  $\sim 120 \text{ K}$  in Fig. 3(b), but the maximum cw efficiency is estimated to be achievable at  $\sim 80 \text{ K}$  as the internal heating for cw operation ( $\sim 16 \text{ K cm}^2/\text{kA}$ ) is not negligible. To maximally profit from the self-heating of the QCL, we set the operating temperature to  $80 \text{ K}$ . The emission of the QCL undergoes a slight blueshift from  $\sim 4.97 \mu\text{m}$  to  $\sim 4.8 \mu\text{m}$  (at  $\sim 0.5 \text{ A}$ ), and the threshold current (threshold current density) considerably decreases from  $0.65 \text{ A}$  ( $1.10 \text{ kA/cm}^2$ ) to  $0.22 \text{ A}$  ( $0.37 \text{ kA/cm}^2$ ). Comparing the pulsed and cw L–I curves in Fig. 4(a), it can be found that below

$\sim 1.0 \text{ A}$ , the SE of the cw operation laser is higher than that of the pulsed one. At  $\sim 1.26 \text{ A}$ , their power difference reaches  $\sim 0.5 \text{ W}$  and the cw-WPE comes to the maximum, up to  $\sim 41\%$ . Further increasing the current, the cw-SE is slowly dropping down and is finally below the pulsed SE due to the continuous increase in internal temperature. At  $\sim 2 \text{ A}$ , the cw output power reaches  $\sim 12 \text{ W}$ . This is the highest cw WPE and cw output power for an intersubband semiconductor laser.

To conclude, we reported a redesigned buried ridge processing technique to achieve nearly complete surface planarization for QCLs. The planarized device geometry improves the thermal conduction and reliability and, most importantly, enhances the power and efficiency. High-performance, planarized QCLs delivering cw output power up to  $12 \text{ W}$  with  $\sim 41\%$  WPE at liquid nitrogen temperature and  $\sim 5.6 \text{ W}$  with  $\sim 20\%$  WPE at room temperature are demonstrated. Both the cw output powers and the  $80 \text{ K}$  cw WPE represent

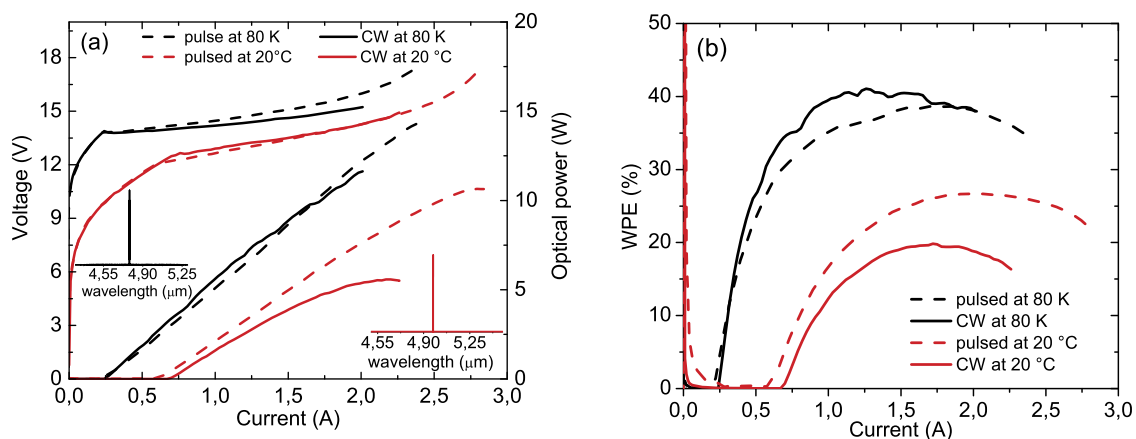


**FIG. 4.** (a) The LIV curves of the QCL working at  $80 \text{ K}$  (black) and  $20^\circ\text{C}$  (red) in pulsed (dashed) and cw (solid) modes, respectively. Inset: the lasing spectra of the QCL at a driving current of  $\sim 0.8 \text{ A}$  at room temperature (red) and at a current of  $\sim 0.5 \text{ A}$  at liquid nitrogen temperature (black). (b) The WPE of the QCL in (a).

significant improvements in the state-of-the-art and strongly extend the efficiency and power capacity of intersubband semiconductor lasers in cw operation.

The authors would like to acknowledge the support and encouragement of the following: Dan Green, Kevin Leonard, Myron Pauli, Jason Auxier, Paul Mak, K. K. Law from Navy, and Mark Rosker from DARPA.

#### DATA AVAILABILITY

The data that support the findings of this study are available from the corresponding author upon reasonable request.

#### REFERENCES

- <sup>1</sup>J. Faist, *Quantum Cascade Lasers* (OUP, Oxford, 2013).
- <sup>2</sup>M. Razeghi, *Vacuum* **146**, 308 (2017).
- <sup>3</sup>M. Razeghi, W. J. Zhou, S. Slivken, Q. Y. Lu, D. H. Wu, and R. McClintock, *Appl. Opt.* **56**, H30 (2017).
- <sup>4</sup>R. Kohler, *Nature* **417**, 156 (2002).
- <sup>5</sup>N. Bandyopadhyay, Y. Bai, B. Gokden, A. Myzaferi, S. Tsao, S. Slivken, and M. Razeghi, *Appl. Phys. Lett.* **97**, 131117 (2010).
- <sup>6</sup>W. Zhou, Q.-Y. Lu, D.-H. Wu, S. Slivken, and M. Razeghi, *Opt. Express* **27**, 15776 (2019).
- <sup>7</sup>Y. Bai, N. Bandyopadhyay, S. Tsao, S. Slivken, and M. Razeghi, *Appl. Phys. Lett.* **98**, 181102 (2011).
- <sup>8</sup>A. Lyakh, M. Suttinger, R. Go, P. Figueiredo, and A. Todi, *Appl. Phys. Lett.* **109**, 121109 (2016).
- <sup>9</sup>M. Razeghi, *IEEE J. Sel. Top. Quantum Electron.* **15**, 941 (2009).
- <sup>10</sup>Y. Bai, S. Slivken, S. Kuboya, S. R. Darvish, and M. Razeghi, *Nat. Photonics* **4**, 99 (2010).
- <sup>11</sup>K. Fujita, M. Yamanishi, T. Edamura, A. Sugiyama, and S. Furuta, *Appl. Phys. Lett.* **97**, 201109 (2010).
- <sup>12</sup>K. Fujita, M. Yamanishi, S. Furuta, A. Sugiyama, and T. Edamura, *Appl. Phys. Lett.* **101**, 181111 (2012).
- <sup>13</sup>D. Botez, J. C. Shin, J. Kirch, C. Chang, L. Mawst, and T. Earles, *IEEE J. Sel. Top. Quantum Electron.* **19**, 1200312 (2013).
- <sup>14</sup>D. Botez, C.-C. Chang, and L. J. Mawst, *J. Phys. D: Appl. Phys.* **49**, 043001 (2016).
- <sup>15</sup>Y. Bai, N. Bandyopadhyay, S. Tsao, E. Selcuk, S. Slivken, and M. Razeghi, *Appl. Phys. Lett.* **97**, 251104 (2010).
- <sup>16</sup>P. Q. Liu, A. J. Hoffman, M. D. Escarra, K. J. Franz, J. B. Khurgin, Y. Dikmelik, X. Wang, J.-Y. Fan, and C. F. Gmachl, *Nat. Photonics* **4**, 95 (2010).